UC Riverside

UC Riverside Previously Published Works

Title

Localization of cortical tissue optical changes during seizure activity in vivo with optical coherence tomography

Permalink

https://escholarship.org/uc/item/3zt745zq

Journal

Biomedical Optics Express, 6(5)

ISSN

2156-7085

Authors

Eberle, Melissa M
Hsu, Mike S
Rodriguez, Carissa L
et al.

Publication Date

2015-05-01

DOI

10.1364/boe.6.001812

Peer reviewed

eScholarship.org Powered by the California Digital Library
University of California

Biomedical Optics EXPRESS

Localization of cortical tissue optical changes during seizure activity *in vivo* with optical coherence tomography

Melissa M. Eberle,[1] Mike S. Hsu,[2] Carissa L. Rodriguez,[1] Jenny I. Szu,[2] Michael C. Oliveira,[1] Devin K. Binder,[2] and B. Hyle Park[1,*]

[1]*Department of Bioengineering, University of California, Riverside, 900 University Ave. Riverside, CA 92521, USA*
[2]*Division of Biomedical Sciences, University of California, Riverside, 900 University Ave. Riverside, CA 92521, USA*
**hylepark@engr.ucr.edu*

Abstract: Optical coherence tomography (OCT) is a high resolution, minimally invasive imaging technique, which can produce depth-resolved cross-sectional images. In this study, OCT was used to detect changes in the optical properties of cortical tissue *in vivo* in mice during the induction of global (pentylenetetrazol) and focal (4-aminopyridine) seizures. Through the use of a confidence interval statistical method on depth-resolved volumes of attenuation coefficient, we demonstrated localization of regions exhibiting both significant positive and negative changes in attenuation coefficient, as well as differentiating between global and focal seizure propagation.

©2015 Optical Society of America

OCIS codes: (110.4500) Optical coherence tomography; (170.3880) Medical and biological imaging; (100.2960) Image analysis.

References and links

1. E. M. C. Hillman, "Optical brain imaging in vivo: techniques and applications from animal to man," J. Biomed. Opt. **12**(5), 051402 (2007).
2. D. N. Lenkov, A. B. Volnova, A. R. D. Pope, and V. Tsytsarev, "Advantages and limitations of brain imaging methods in the research of absence epilepsy in humans and animal models," J. Neurosci. Methods **212**(2), 195–202 (2013).
3. S. A. Boppart, "Optical coherence tomography: technology and applications for neuroimaging," Psychophysiology **40**(4), 529–541 (2003).
4. P. G. Aitken, D. Fayuk, G. G. Somjen, and D. A. Turner, "Use of intrinsic optical signals to monitor physiological changes in brain tissue slices," Methods **18**(2), 91–103 (1999).
5. S. Bahar, M. Suh, M. Zhao, and T. H. Schwartz, "Intrinsic optical signal imaging of neocortical seizures: the 'epileptic dip'," Neuroreport **17**(5), 499–503 (2006).
6. P. Federico, S. G. Borg, A. G. Salkauskus, and B. A. MacVicar, "Mapping patterns of neuronal activity and seizure propagation by imaging intrinsic optical signals in the isolated whole brain of the guinea-pig," Neuroscience **58**(3), 461–480 (1994).
7. D. M. Rector, K. M. Carter, P. L. Volegov, and J. S. George, "Spatio-temporal mapping of rat whisker barrels with fast scattered light signals," Neuroimage **26**(2), 619–627 (2005).
8. M. R. Hajihashemi, T. Zhang, B. K. Ormerod, and H. Jiang, "Non-invasive detection of optical changes elicited by seizure activity using time-series analysis of light scattering images in a rat model of generalized seizure," J. Neurosci. Methods **227**, 18–28 (2014).
9. J. Yang, T. Zhang, H. Yang, and H. Jiang, "Fast multispectral diffuse optical tomography system for in vivo three-dimensional imaging of seizure dynamics," Appl. Opt. **51**(16), 3461–3469 (2012).
10. T. Zhang, J. Zhou, R. Jiang, H. Yang, P. R. Carney, and H. Jiang, "Pre-seizure state identified by diffuse optical tomography," Sci. Rep. **4**, 3798 (2014).
11. J. R. Weber, M. Hsu, A. Lin, D. Lee, C. Owen, D. K. Binder, D. J. Cuccia, A. J. Durkin, and B. J. Tromberg, "Noncontact imaging of seizures using multispectral spatial frequency domain imaging," in *OSA BIOMED* (2010).
12. M. Choma, M. Sarunic, C. Yang, and J. Izatt, "Sensitivity advantage of swept source and Fourier domain optical coherence tomography," Opt. Express **11**(18), 2183–2189 (2003).
13. J. F. de Boer, B. Cense, B. H. Park, M. C. Pierce, G. J. Tearney, and B. E. Bouma, "Improved signal-to-noise ratio in spectral-domain compared with time-domain optical coherence tomography," Opt. Lett. **28**(21), 2067–2069 (2003).

#234156 - $15.00 USD Received 9 Feb 2015; revised 10 Apr 2015; accepted 16 Apr 2015; published 22 Apr 2015

14. D. Huang, E. A. Swanson, C. P. Lin, J. S. Schuman, W. G. Stinson, W. Chang, M. R. Hee, T. Flotte, K. Gregory, C. A. Puliafito, and J. G. Fujimoto, "Optical Coherence Tomography," Science **254**(5035), 1178–1181 (1991).
15. R. Leitgeb, W. Drexler, A. Unterhuber, B. Hermann, T. Bajraszewski, T. Le, A. Stingl, and A. Fercher, "Ultrahigh resolution Fourier domain optical coherence tomography," Opt. Express **12**(10), 2156–2165 (2004).
16. J. M. Schmitt, "Optical coherence tomography (OCT): a review," IEEE J. Sel. Top. Quantum Electron. **5**(4), 1205–1215 (1999).
17. S. Yun, G. Tearney, B. Bouma, B. Park, and J. de Boer, "High-speed spectral-domain optical coherence tomography at 1.3 mum wavelength," Opt. Express **11**(26), 3598–3604 (2003).
18. B. Park, M. C. Pierce, B. Cense, S. H. Yun, M. Mujat, G. Tearney, B. Bouma, and J. de Boer, "Real-time fiber-based multi-functional spectral-domain optical coherence tomography at 1.3 μm," Opt. Express **13**(11), 3931–3944 (2005).
19. Y. Chen, A. D. Aguirre, L. Ruvinskaya, A. Devor, D. A. Boas, and J. G. Fujimoto, "Optical coherence tomography (OCT) reveals depth-resolved dynamics during functional brain activation," J. Neurosci. Methods **178**(1), 162–173 (2009).
20. M. M. Eberle, C. L. Reynolds, J. I. Szu, Y. Wang, A. M. Hansen, M. S. Hsu, M. S. Islam, D. K. Binder, and B. H. Park, "In vivo detection of cortical optical changes associated with seizure activity with optical coherence tomography," Biomed. Opt. Express **3**(11), 2700–2706 (2012).
21. B. W. Graf, T. S. Ralston, H. J. Ko, and S. A. Boppart, "Detecting intrinsic scattering changes correlated to neuron action potentials using optical coherence imaging," Opt. Express **17**(16), 13447–13457 (2009).
22. S. W. Jeon, M. A. Shure, K. B. Baker, D. Huang, A. M. Rollins, A. Chahlavi, and A. R. Rezai, "A feasibility study of optical coherence tomography for guiding deep brain probes," J. Neurosci. Methods **154**(1-2), 96–101 (2006).
23. U. M. Rajagopalan and M. Tanifuji, "Functional optical coherence tomography reveals localized layer-specific activations in cat primary visual cortex in vivo," Opt. Lett. **32**(17), 2614–2616 (2007).
24. R. U. Maheswari, H. Takaoka, H. Kadono, R. Homma, and M. Tanifuji, "Novel functional imaging technique from brain surface with optical coherence tomography enabling visualization of depth resolved functional structure in vivo," J. Neurosci. Methods **124**(1), 83–92 (2003).
25. M. Sato, D. Nomura, T. Tsunenari, and I. Nishidate, "In vivo rat brain measurements of changes in signal intensity depth profiles as a function of temperature using wide-field optical coherence tomography," Appl. Opt. **49**(30), 5686–5696 (2010).
26. Y. Satomura, J. Seki, Y. Ooi, T. Yanagida, and A. Seiyama, "In vivo imaging of the rat cerebral microvessels with optical coherence tomography," Clin. Hemorheol. Microcirc. **31**(1), 31–40 (2004).
27. V. Tsytsarev, B. Rao, K. I. Maslov, L. Li, and L. V. Wang, "Photoacoustic and optical coherence tomography of epilepsy with high temporal and spatial resolution and dual optical contrasts," J. Neurosci. Methods **216**(2), 142–145 (2013).
28. M. Lazebnik, D. L. Marks, K. Potgieter, R. Gillette, and S. A. Boppart, "Functional optical coherence tomography for detecting neural activity through scattering changes," Opt. Lett. **28**(14), 1218–1220 (2003).
29. K. Bizheva, A. Unterhuber, B. Hermann, B. Povazay, H. Sattmann, W. Drexler, A. Stingl, T. Le, M. Mei, R. Holzwarth, H. A. Reitsamer, J. E. Morgan, and A. Cowey, "Imaging ex vivo and in vitro brain morphology in animal models with ultrahigh resolution optical coherence tomography," J. Biomed. Opt. **9**(4), 719–724 (2004).
30. S. A. Boppart, B. E. Bouma, M. E. Brezinski, G. J. Tearney, and J. G. Fujimoto, "Imaging developing neural morphology using optical coherence tomography," J. Neurosci. Methods **70**(1), 65–72 (1996).
31. K. A. Vermeer, J. Mo, J. J. A. Weda, H. G. Lemij, and J. F. de Boer, "Depth-resolved model-based reconstruction of attenuation coefficients in optical coherence tomography," Biomed. Opt. Express **5**(1), 322–337 (2013).
32. J. I. Szu, M. M. Eberle, C. L. Reynolds, M. S. Hsu, Y. Wang, C. M. Oh, M. S. Islam, B. H. Park, and D. K. Binder, "Thinned-skull cortical window technique for in vivo optical coherence tomography imaging," J. Vis. Exp. **69**, e50053 (2012).
33. D. K. Binder, K. Oshio, T. Ma, A. S. Verkman, and G. T. Manley, "Increased seizure threshold in mice lacking aquaporin-4 water channels," Neuroreport **15**(2), 259–262 (2004).
34. C. L. R. Rodriguez, J. I. Szu, M. M. Eberle, Y. Wang, M. S. Hsu, D. K. Binder, and B. H. Park, "Decreased light attenuation in cerebral cortex during cerebral edema detected using optical coherence tomography," Neurophotonics **1**(2), 025004 (2014).
35. M. Zhao, H. Ma, M. Suh, and T. H. Schwartz, "Spatiotemporal dynamics of perfusion and oximetry during ictal discharges in the rat neocortex," J. Neurosci. **29**(9), 2814–2823 (2009).
36. M. Zhao, J. Nguyen, H. Ma, N. Nishimura, C. B. Schaffer, and T. H. Schwartz, "Preictal and ictal neurovascular and metabolic coupling surrounding a seizure focus," J. Neurosci. **31**(37), 13292–13300 (2011).
37. Y. Wang, C. M. Oh, M. C. Oliveira, M. S. Islam, A. Ortega, and B. H. Park, "GPU accelerated real-time multi-functional spectral-domain optical coherence tomography system at 1300 nm," Opt. Express **20**(14), 14797–14813 (2012).
38. M. Mujat, B. H. Park, B. Cense, T. C. Chen, and J. F. de Boer, "Autocalibration of spectral-domain optical coherence tomography spectrometers for in vivo quantitative retinal nerve fiber layer birefringence determination," J. Biomed. Opt. **12**(4), 041205 (2007).

#234156 - $15.00 USD Received 9 Feb 2015; revised 10 Apr 2015; accepted 16 Apr 2015; published 22 Apr 2015
(C) 2015 OSA

1. Introduction

High resolution and minimally-invasive imaging techniques have been vital in understanding and visualizing the functionality of the brain *in vivo* [1–3]. Clinical imaging techniques such as functional magnetic imaging (fMRI), positron emission tomography (PET), and computed tomography (CT) are widely used in investigating the structure and function of the brain, but have limitations with regards to image resolution, acquisition speed, and specificity [1,2]. Optical imaging techniques such as intrinsic optical signal (IOS) [4–7], diffuse optical tomography (DOT) [8–10], and spatial frequency domain imaging (SFDI) [11] overcome these limitations by achieving high-resolution, minimally invasive, imaging of the occurrence and propagation of neuronal and epileptic activity through changes in intrinsic tissue optical properties.

Optical coherence tomography (OCT) is a label-free, high-resolution, noncontact imaging technique, capable of producing depth-resolved, cross-sectional, three-dimensional (3D) volumes [12–18] and has been shown to be a promising method for *in vivo* imaging in highly scattering tissues such as the cerebral cortex [19–30]. We previously identified changes in the intensity of the cortex during the progression of induced generalized seizures *in vivo* in mice with OCT [20]. From each cross-sectional image, the average image intensity was calculated from a large region of interest, spanning 4 mm in the sagittal plane of the cerebral cortex and 1.5 mm in depth. By analyzing the temporal changes of these values, we observed significant decreases in the average intensity of cortical tissue preceding and during generalized tonic-clonic seizures induced with pentylenetetrazol (PTZ) [20].

The objective of this study was to expand on our previous findings by utilizing the spatiotemporal resolution of OCT in order to localize changes in the optical properties of murine cerebral cortex during seizure progression *in vivo* in both a global model (PTZ) and a focal model (4-aminopyridine (4-AP)), which is known to induce localized seizures at the site of 4-AP injection. Sequential volumetric scans of the cortex were acquired for both global and focal animal models and the spatiotemporal progression of the percent change in intensity was determined highlighting the differences in seizure propagation between the two models.

To mitigate any contributions from the imaging system to changes in the observed optical parameters, a recently published method for determining per-pixel depth-resolved tissue attenuation coefficients was used [31]. We then applied a confidence interval statistical analysis method to further quantify and localize regions within the attenuation volumes with significant changes during the progression of both seizure models. With our functional OCT (*f*OCT) volumes, we were able to visualize and further localize the spatiotemporal propagation of the attenuation changes through the cortical tissue.

2. Materials and experimental methods

2.1 Animal preparation for in vivo experimentation

Adult female (>6 weeks of age) CD1 mice were anesthetized with urethane (1.5 mg/g). The animals were then placed into a standard rodent stereotactic frame. Animals were kept on a heating blanket to maintain normal body temperature throughout the experiment. Anesthesia was maintained using a Ketamine/Xylazine mixture (80 mg/kg Ketamine, 10 mg/kg Xylazine) intraperitoneally (i.p.). Eight animals were used: two for the global model and six for the focal model (two control and four experimental). All experimental procedures were approved by the University of California, Riverside Institutional Animal Care and Use Committee.

2.1.1 Global seizure model

A 4 x 4 mm thinned skull cortical window was created with a dental bur over the cerebral cortex in the right hemisphere [32]. The skull was thinned to an approximately 55 μm throughout the window. OCT volumetric data was collected prior to i.p. injection of PTZ (100 mg/kg) and was collected through the entire experiment with an imaging window of 4 x 2

#234156 - $15.00 USD Received 9 Feb 2015; revised 10 Apr 2015; accepted 16 Apr 2015; published 22 Apr 2015
(C) 2015 OSA

mm. PTZ is a $GABA_A$ antagonist that reproducibly causes generalized seizures in this mouse model with a latency after injection [33]. Once a generalized tonic-clonic (stage-5) seizure was observed, involving fore- and hind-limb twitches and tail movement, the animal was sacrificed with an anesthesia overdose. Internal control measurements, prior to PTZ injection, were acquired with a 10 min baseline and 20 min post i.p. injection of saline (100 mg/kg). More extensive controls showed no significant change over 80 min in the same animal model with an $n = 3$ [34].

2.1.2 Focal seizure model

While the use of a thin skull cortical window better preserves the natural state of the brain, localized injections of 4-AP, a potassium channel blocker known to cause acute focal seizures at the injection site [5,35,36], required partial removal of the skull. After anesthesia induction, a linear midline skin incision was made on the scalp. A hemicraniectomy was performed to remove the bone between coronal suture and the lambdoidal suture. Animals then received intracerebral injections of 4-AP (15 mM) at a rate of 50 nl per minute for 10 minutes to induce focal seizures. The pipette was placed 0.5 mm into the cortical tissue and positioned 1.5 mm lateral and 1.0 mm caudal relative to bregma. The pipettes were custom pulled from 3.5" capillaries with a tip dimension of approximately 300 μm. OCT volumetric data was acquired through the entire experiments. The first two of the six animals were imaged with a 3 x 3 mm imaging window directly at the injection site to ensure we observed any possible changes in intensity and attenuation during the focal seizure. Once we verified that we could in fact visualize these changes, we widened the imaging window to a 5 x 4 mm imaging window covering the hemicraniectomy region for the next four animals to visualize the spatial propagation of the changes from the site of injection. For the control experiment, artificial cerebrospinal fluid (ASCF) was substituted for the 4-AP injections.

2.2 Spectral-domain optical coherence tomography (SD-OCT)

The SD-OCT system [37] (Fig. 1) utilized a broadband source composed of two super-luminescent diodes (SLD), one centered at 1295nm with a full-width at half maximum (FWHM) bandwidth of 97 nm (Thorlabs Inc.) and the other centered at 1350 nm with a FWHM bandwidth of 48 nm (Denselight Semiconductors Pte Ltd). The combined source was centered at 1298 nm with a 120 nm FWHM bandwidth. The experimentally determined axial and lateral resolutions were 8 μm and 20 μm respectively. From the source, the light was sent to a fiber circulator (Thorlabs Inc.) and split with an 80/20 fiber coupler between the sample and reference arm. In the sample arm, a pair of galvanometer (gm) mirrors provided transverse scanning of a 10 μm diameter focused beam. The lens used to direct light to the sample (AC254-075-C, ThorLabs) had a 1 inch diameter with a focal length of 75 mm. The reflected light from both arms was then recombined at the splitter and the now interfered light was sent to a spectrometer with a transmission diffraction grating (1100 lines per mm, Wasatch Photonics) before being focused by a planoconvex lens onto a 1024 pixel line scan camera (lsc, Goodrich SUI SU-LDH linear digital high speed InGaAs camera).

#234156 - $15.00 USD Received 9 Feb 2015; revised 10 Apr 2015; accepted 16 Apr 2015; published 22 Apr 2015
(C) 2015 OSA

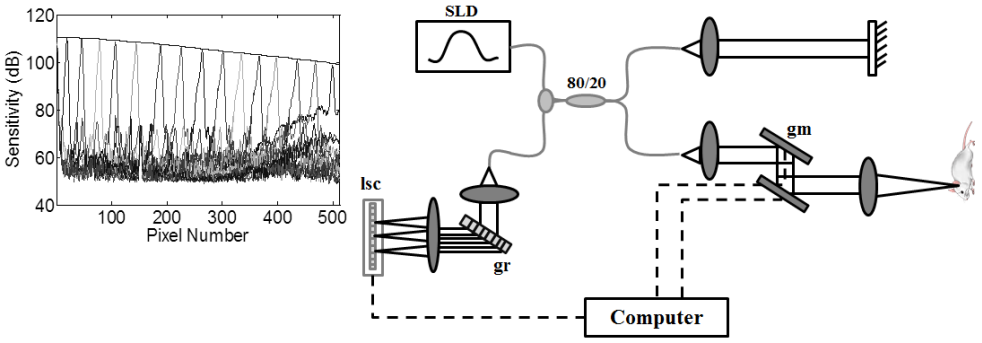

Fig. 1. Schematic of the SD-OCT system. SLD: superluminescent diode, lsc: line scan camera, gm: galvanometer, gr: grating. Graph inset is the spectrometer roll-off demonstrating an 11 dB loss over the maximum imaging depth.

2.3 Image acquisition and OCT data processing

OCT volumetric data acquisition was performed with axial depth profiles (A-lines) acquired at 15 kHz. Two different acquisition protocols were used to either optimize the spatial or temporal resolution. To optimize the spatial resolution, a single volume of 200 sagittal cross-sectional images composed of 2048 A-lines was acquired every 2 minutes. To optimize the temporal resolution, a single volume of 150 images composed of 512 A-lines was acquired every 40 s. In either case, an imaging depth of 2 mm was obtained with 6 mW of incident power with a focal point 1 mm below the cortical surface. To correct for the nonlinear *k*-space sampling of the spectral data, 512 sampled points per A-line scan were mapped to uniform wavenumber spacing by linear interpolation [38]. The fast Fourier-transformation (FFT) from wavenumber to spatial domain was performed as well as secondary image processing, including plotting the intensity images on a logarithmic inverse gray scale [37]. The depth-dependent sensitivity of SD-OCT acquisition was measured (Fig. 1) and then removed by multiplying each A-line by a calculated correction curve [17,18] to yield adjusted intensity images, a correction step necessary for accurate depth-dependent attenuation coefficient calculations [31]. After the initial OCT image processing, gross registration of sequential volumes was performed by maximizing the three-dimensional cross-correlation with the initial volume of each data set. This ensured accurate registration of the volumes throughout the experiment through the calculation and verification of high correlation coefficients. Our images had a maximum SNR of 35 dB and the following analysis was performed on regions with an SNR of at least 10 dB.

2.4 Depth-resolved attenuation coefficient volumes

A median filter of 64 x 64 μm was applied to minimize variations due to coherent speckle. This kernel size was determined starting from a cross-sectional area based on the lateral and axial resolutions, and iteratively expanded to determine the minimum cross-sectional area required to achieve a speckle contrast ratio below 0.1 over a region of uniform cortical tissue. We then calculated depth-resolved, per-pixel attenuation coefficient values (μ) (Fig. 2) for each volume using the algorithm described by Vermeer *et al.* [31]. The attenuation coefficients found for gray and white matter ranged between 1 and 4 mm^{-1} and 4-8 mm^{-1}, respectively, and are comparable to previously published data [22,34].

#234156 - $15.00 USD Received 9 Feb 2015; revised 10 Apr 2015; accepted 16 Apr 2015; published 22 Apr 2015
(C) 2015 OSA

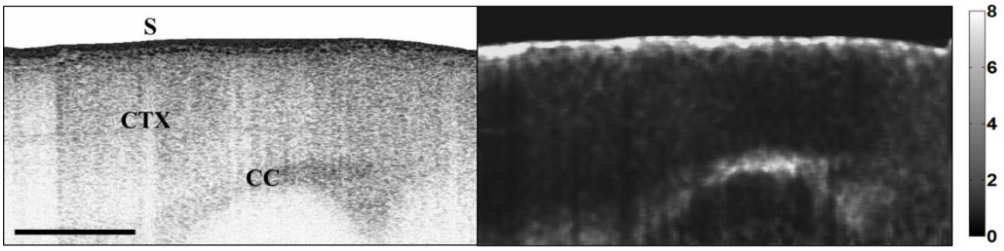

Fig. 2. Intensity (left) and the corresponding attenuation coefficient (right) sagittal image of mouse brain tissue. Color bar represents μ in units of mm^{-1}. S: skull, CTX: cerebral cortex and CC: corpus callosum. Bar: 1mm

A confidence interval (C.I.) analysis was used in order to highlight only the attenuation values that represent a statistically significant deviation outside the range of natural variations in attenuation. Baseline volumetric data acquired prior to seizure initiation was used to generate the confidence intervals with the mean ($\bar{x}$) and standard error (SE) calculated from 30 x 30 x 30 μm voxels. The SEs were calculated from the sample standard deviation in each voxel (*s*) and the number of baseline volumes (*n*). The confidence level (0.90 or 0.95) chosen for each experiment's C.I. analysis was based on the baseline degrees of freedom (*df*), defined as (*n* - 1), dictating which *t** value was selected to ensure a similar t-distribution for all experiments.

$$C.I. = \bar{x} \pm t^{*} SE, SE = s / \sqrt{n}$$

Once the boundaries of the C.I.s were determined, the mean in each voxel ($\bar{x}$) for each post-baseline volume was compared to the C.I. defined for the voxel. If the mean value fell above or below the C.I., then the percent change from maximum or minimum, respectively, of the C.I. was calculated as

$$\Delta\mu = 100 \times \left(\bar{x}(x,y,z,t) - CI_{max,min}(x,y,z) \right) \Big/ CI_{max,min}(x,y,z)$$

and assigned to the voxel, creating volumes of percent change in attenuation coefficient while maintaining the spatial specificity of μ in the cortical tissue. As a result, time points where the mean attenuation value was within the C.I. for a given voxel are made visually distinct from those that were statistically significantly above (red) or below (blue) this normative range.

3. Results

3.1 Changes in intensity during global and focal seizures

Control experiments were performed for both global and focal seizure models. To optimize the spatial resolution, a single volume of 200 sagittal cross-sectional images composed of 2048 A-lines was acquired every 2 minutes. We acquired 4 x 2 mm volumes and 3 x 3 mm volumes for the global and focal experiments respectively. After the collection of baseline volumes, the injection of either saline (global) or ACSF (focal) was administered. The timing of the injections is shown in Fig. 3 along with the percent change in average intensity from selected 0.5 x 0.5 x 0.5 mm regions of interest (ROIs). Figure 3(A) shows two representative ROIs that were 1 mm lateral from each other and 1 mm from both the anterior and posterior of the volume. It should be noted that a total of 5 ROIs were analyzed in each set of data, with all exhibiting similar behavior. For the focal experiments (Fig. 3(B)), ROIs were selected at the injection site and 1 mm lateral and 2 mm posterior from the injection site. The mean of the baseline data in each model was used to calculate a two standard deviation (2SD) in the intensity change of ± 2% for the global model (Fig. 3(A)) and ± 3% for the focal model (Fig.

#234156 - $15.00 USD Received 9 Feb 2015; revised 10 Apr 2015; accepted 16 Apr 2015; published 22 Apr 2015
(C) 2015 OSA

3(B)), plotted as red, horizontal, dashed lines in Fig. 3, indicating the intrinsic fluctuation in the intensity values. The trend in the percent change in intensity stayed within the 2SD throughout the experiments for both the global and the focal models (Fig. 3).

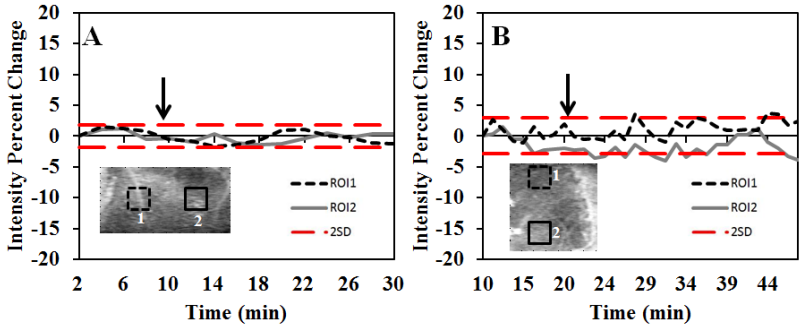

Fig. 3. Percent change in average intensity for (A) Global and (B) Focal controls 0.5 x 0.5 x 0.5 mm ROIs. Global ROIs are separated 1 mm laterally outlined on the *en face* intensity image. Focal ROIs are located at the injection site (ROI 2) and 2 mm from the injection site (ROI 1) outlined on the *en face* intensity image. Arrows represent time of injection. Red horizontal bars: 2SD of the baseline mean. *En face* insets of a reference intensity volume. Top of image: Bregma, left of image: Rostral.

Global and focal *in vivo* seizure experiments were conducted and in order to determine the changes in intensity during seizure progression from a pre-seizure state, an average baseline volume was calculated from five volumes (global) or three volumes (focal). The fractional intensity change of each following volume was computed by pointwise division of each volume by the average baseline volume. The square of the logarithm of the fractional changes were then computed in order to better visualize all changes in intensity from baseline, with the sign of the original logarithm reapplied after squaring. The ratio values in each pixel were scaled from black to color saturation at a predetermined threshold value that represented a greater than ± 50% change from baseline (blue represented ratios below baseline and red represented ratios above baseline) (Figs. 4 and 5). Three dimensional (3D) volumetric renderings of the spatiotemporal changes in intensity during both global (Fig. 4) and focal (Fig. 5) seizure progression were generated using Amira (FEI Visualization Sciences Group).

A representative result of the progression of changes in intensity can be seen in the rendered volumes following PTZ injection shown in Fig. 4. Twenty-six minutes post injection, a significantly large decrease in intensity is apparent due to the accumulation of blue pixels throughout the imaged cortical tissue. The global nature of the decrease verifies the generalized nature of PTZ seizure progression. Representative results in Fig. 5 from the focal seizure experiments show the progression of the intensity changes from the injection site, which is outlined in white at minute 12, following the last 4-AP injection. At 16 minutes post injections, a region of decreasing intensity initiates at the injection site. The blue pixels continue to accumulate indicating a significant decrease in intensity focused at the site of injection as the seizure continues to progress through the end of the experiment. The data for both the global and focal models were representative and the experiments were successfully repeated with similar results.

#234156 - $15.00 USD Received 9 Feb 2015; revised 10 Apr 2015; accepted 16 Apr 2015; published 22 Apr 2015
(C) 2015 OSA

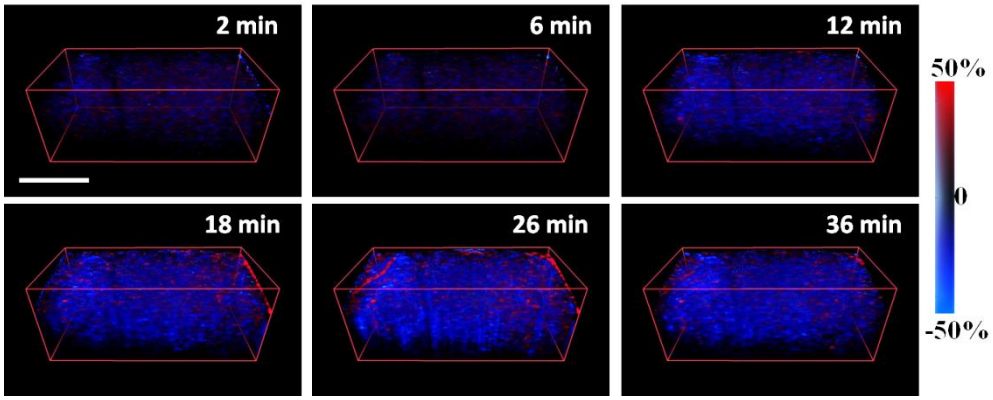

Fig. 4. Volumes of change in intensity for the global seizure model. Volumes are 4 x 2 x 2 mm. Color bar: percent change from baseline (0%) saturating at ± 50%. Time is min post-PTZ injection. Top of image: Bregma, left of image: Rostral. Scale bar: 1 mm. (see Media 1).

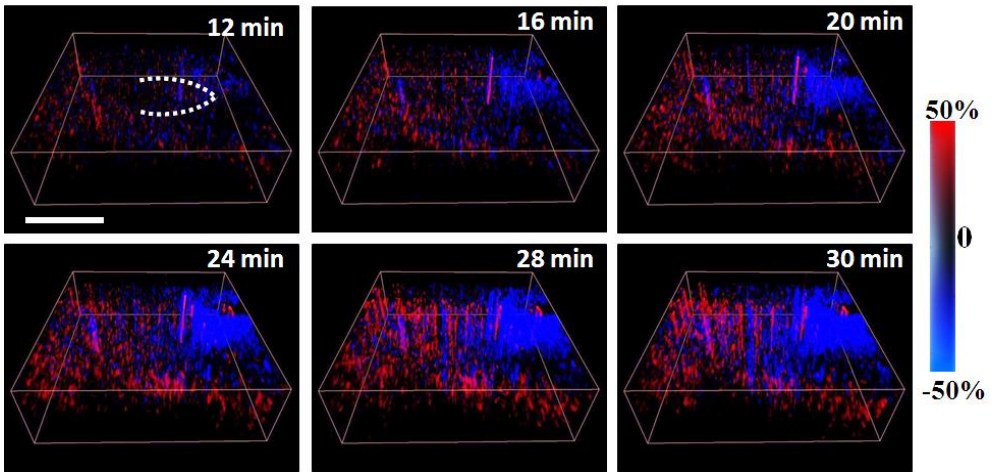

Fig. 5. Volumes of change in intensity for the focal seizure model. Volumes are 3 x 3 x 2 mm. Location of pipette injections is outlined in the first frame. Color bar: percent change from baseline (0%) saturating at ± 50%. Time is min post 4-AP injections. Top of image: Bregma, left of image: Rostral. Scale bar: 1 mm. (see Media 2).

In order to quantifiably differentiate the progression of the changes in intensity between the global and focal model, we analyzed the time course of the average fractional reflectivity from ROIs selected in the same manner as outlined in the control experiments (Fig. 3). Figure 6(A) shows the location of the ROIs within the volume for the global model and both ROIs show mirroring trends of decreasing intensity starting 6-8 min post-PTZ injection and reaching a maximum of 10-15% change from the baseline at full seizure onset 24 min post-PTZ injection. The animals were then given an anesthesia overdose at full seizure, which occurred at minute 29, and the average intensity began to return to baseline by the end of the experiment. In contrast for the focal model, a significant decrease in intensity occurred only in the ROI at the injection site starting 10 min post 4-AP injections, and reached a maximum 41% change 28 min post-injection. The two ROIs away from the injection site show no significant change in intensity outside the 2SD during the experiment. This analysis highlights the difference between the global and focal seizure spatiotemporal progression of changes in intensity during seizure progression.

#234156 - $15.00 USD Received 9 Feb 2015; revised 10 Apr 2015; accepted 16 Apr 2015; published 22 Apr 2015
(C) 2015 OSA

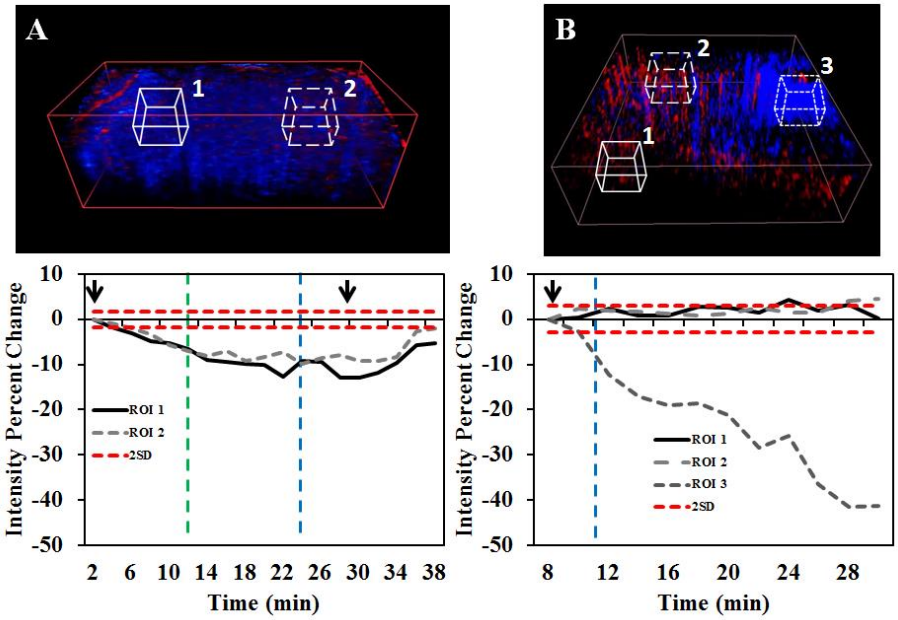

Fig. 6. Global (A) and focal (B) seizure ROI analysis with the location of ROIs within the imaged volume and the intensity percent change plotted vs. time (A) post-PTZ and (B) post 4-AP injections along with each baseline 2SD as red, dashed, horizontal lines. (A) The first arrow is the time of PTZ injection the second is the anesthesia overdose. (B) Arrow is time of last 4-AP injection. The vertical dashed lines indicate stage-2 (green) and stage-5 (blue) seizures respectively. All ROIs are 0.5 x 0.5 x 0.5 mm.

3.2 Changes in attenuation during global and focal seizures

Using the method described in section 2.4, attenuation coefficient volumes were calculated from the intensity volumes for all of the global and focal control and seizure experiments. The same ROIs were used for the control experiments and Fig. 7 shows the percent change in average attenuation values for both the global (Fig. 7A) and the focal (Fig. 7(B)) control experiments. The 2SDs of the baseline means were ± 2.5% for the global model and ± 2% for the focal model, plotted as red, horizontal, dashed lines in Fig. 7, indicating the intrinsic fluctuation in the attenuation values with time. The percent change in attenuation stayed within the 2SD throughout the control experiments for both models.

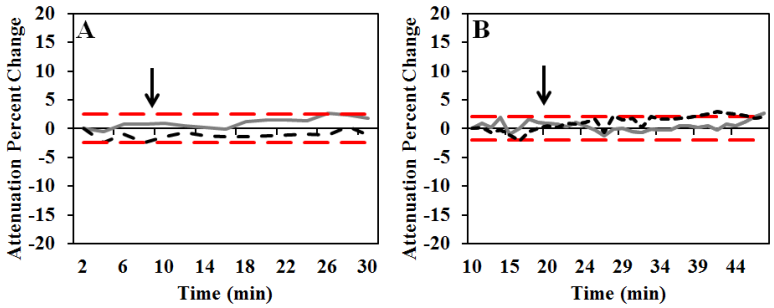

Fig. 7. Percent change in average attenuation for (A) Global and (B) Focal controls 0.5 x 0.5 x 0.5 mm ROIs. Global ROIs are separated 1 mm laterally. Focal ROIs are located at the injection site (solid gray) and 2 mm from the injection site (dashed black). Arrows represent time of injection. Red horizontal bars: 2SD of the baseline mean.

#234156 - $15.00 USD Received 9 Feb 2015; revised 10 Apr 2015; accepted 16 Apr 2015; published 22 Apr 2015
(C) 2015 OSA

Figure 8 and 9 shows the total count of attenuation values in three different layers of the cortical tissue: Layer A was the top 65 μm under the surface, layer B was the following 52 μm, and layer C was the following 130 μm. Layer thicknesses were determined based on visual inspection of Δμ patterns visible in the *f*OCT volumes in Figs. 10 and 11. The left graphs are the baseline distribution of attenuation values and the right graphs are the post seizure distribution of attenuation values.

When conducting the global seizure experiments, five volumes were acquired prior to PTZ injection providing a *df* of four, allowing for the use of a 0.95 confidence level. The black line outlined on the histograms in Fig. 8 represents the binned counts of attenuation coefficient values within the calculated 0.95 confidence level for each of the three distinct layers. From these parameters and the five baseline volumes, a C.I. for each 30 x 30 x 30 μm voxel was calculated using the method described in section 2.4.

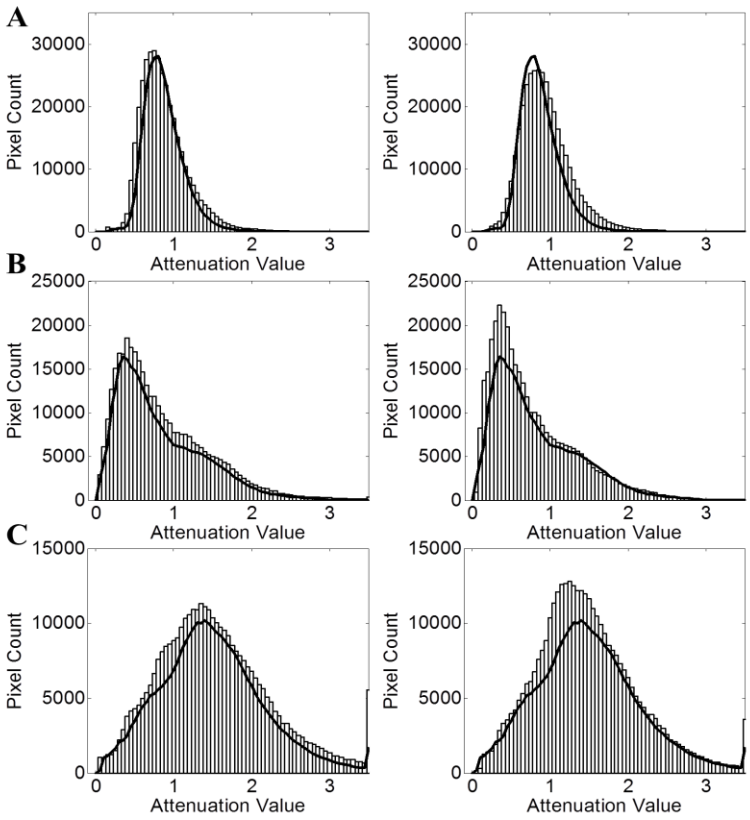

Fig. 8. Histograms of the attenuation value distribution in three layers of the cortical tissue in a global model experiment for baseline (Left) and post seizure onset (Right). The black line is the baseline attenuation values that formed the 0.95 confidence level. Layer (A) top 65 μm, layer (B) following 52 μm, and layer (C) following 130 μm.

For the first set of focal experiments (3 x 3 x 2 mm volumes), the C.I. formation, as seen in Fig. 9, was similar to the global experiments except only three volumes, which were acquired post 4-AP injections but prior to seizure onset, were used to form the baseline data set. Due to the fact that this provided a *df* of only two, the use of a 0.90 confidence level was required. Tissue deformation resulting from the injections inhibited the use of earlier volumes. The left graphs in Fig. 9 are the baseline distribution of attenuation values and the right graphs are the post seizure distribution with each layer's 0.90 confidence level displayed as the black line.

#234156 - $15.00 USD Received 9 Feb 2015; revised 10 Apr 2015; accepted 16 Apr 2015; published 22 Apr 2015
(C) 2015 OSA

When comparing the distribution changes in attenuation values between baseline and post seizure as well as between global and focal seizure models, it is apparent that in the focal model there is a distinct difference between the three layers. The distribution of the top layer (Fig. 9(A)) shifts to the right post seizure, indicating a significant increase in the attenuation values while the middle layer (Fig. 9(B)) shows very little shift and the bottom layer (Fig. 9(C)) shows a large shift to the left indicating a significant decrease in the attenuation values. In the focal seizure there is a layer dependent change in attenuation where the global model (Fig. 8) shows significant deviations from the defined confidence level line, but no layer dependent directionality to the changes.

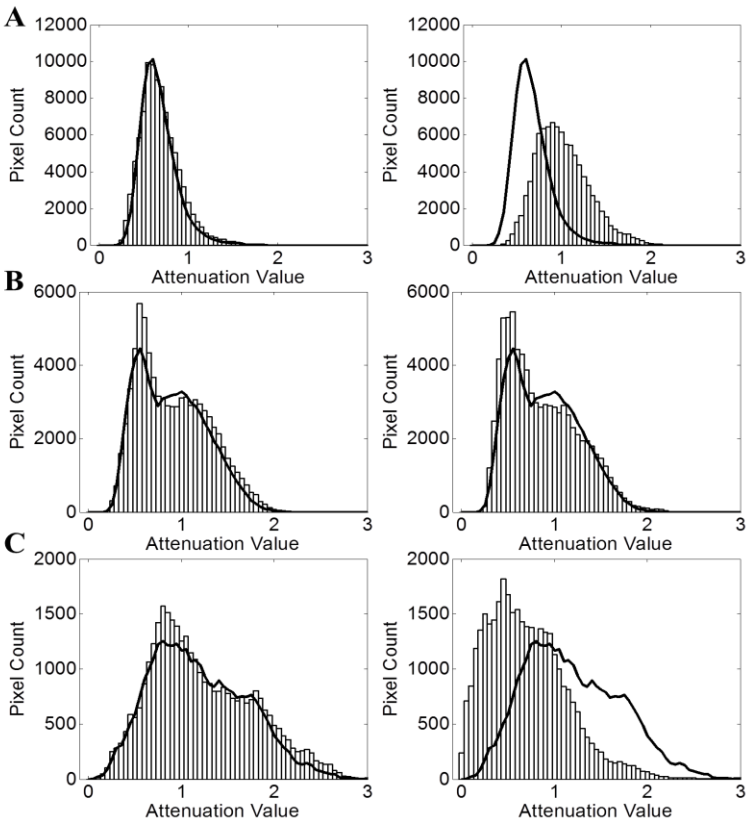

Fig. 9. Histograms of the attenuation value distribution in three layers of the cortical tissue in a focal model experiment for baseline (Left) and post seizure onset (Right). The black line is the baseline attenuation values that formed the 0.90 confidence level. Layer (A) top 65 μm, layer (B) following 52 μm, and layer (C) following 130 μm.

3.3 Visualization of fOCT volumes for global and focal seizure progression

In order to visualize the spatial distribution of the changes in attenuation coefficient for both the global and focal seizure models, 3D *f*OCT volumes [19,21,23,24] were created. As defined in section 2.4, for each voxel in every volume post baseline, a $\Delta\mu$ above or below the C.I. was calculated and then each voxel was assigned a color ranging from black to color saturation, at a maximum percent change threshold, with gradations of red representing voxels of percent change above the C.I. and gradations of blue representing voxels of percent change below the C.I.

#234156 - $15.00 USD Received 9 Feb 2015; revised 10 Apr 2015; accepted 16 Apr 2015; published 22 Apr 2015
(C) 2015 OSA

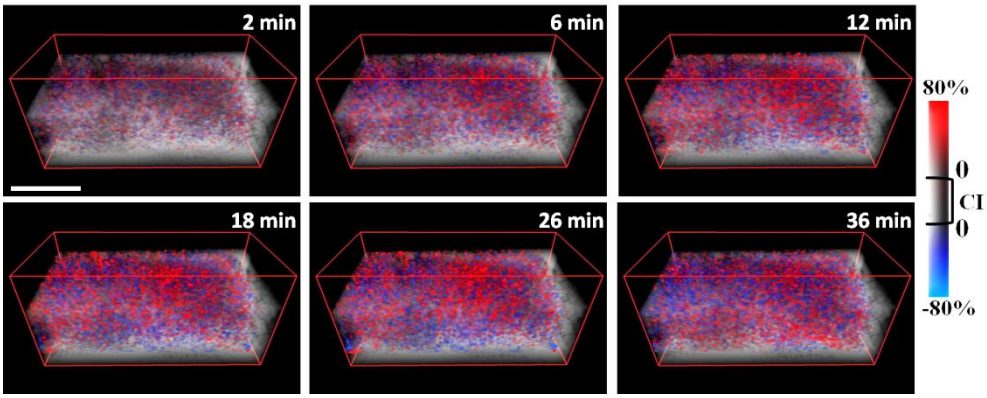

Fig. 10. *f*OCT volumes of the global seizure 4 x 2 x 2 mm. Color is scaled from black to color saturation at −80% Δμ for blue and 80% Δμ for red representing decreased and increased Δμ respectively. *f*OCT volumes are combined with corresponding attenuation coefficient volumes. Time is min post PTZ injection. Top of image: Bregma, left of image: Rostral. Bar: 1 mm. (see Media 3).

Figure 10 shows the global seizure *f*OCT volumes numbered as minutes post PTZ injection with Δμ saturating at ± 80% for both red and blue voxels. We combined the *f*OCT volumes with their corresponding attenuation coefficient volumes to show the precise anatomical registration of the *f*OCT volumes as well as provide a reference to the location of Δμ in the cortical tissue. In the global model, voxels that exhibit both positive and negative Δμ are distributed throughout the imaged tissue. Significant changes in Δμ begin to accumulate throughout the tissue 6 min post PTZ injection and continue through full seizure (24 min), saturating at ± 80% Δμ (Fig. 10). The *f*OCT volumes maintain the spatial distribution of the voxels and eliminate the need for averaging, providing voxel specific Δμ and revealing significant percent changes in attenuation as well as the heterogeneous distribution of both positive and negative Δμ, reflecting the known global nature of seizure progression in the global model.

For the first set of focal model experiments, we acquired 3 x 3 x 2 mm volumes directly at the injection site for optimal spatial resolution during seizure propagation. The resulting *f*OCT volumes are shown in Fig. 11. Each volume is combined with a corresponding attenuation coefficient volume and Δμ is displayed with saturated blue and red voxels at −50% Δμ and 80% Δμ respectively. We extended the red threshold further than the blue to better visualize the distribution of Δμ since the range of positive percent change in attenuation was larger than the negative. *f*OCT volumes provide visualization of depth-dependent changes in attenuation coefficient and the focal nature of the change in tissue attenuation is illustrated in Fig. 11. At the surface of the cortical tissue, a significant increase in Δμ is visible, beginning to coalesce starting at 20 min post-4-AP injections. Directly below, there is a corresponding region where Δμ significantly decreases through focal seizure onset, initiating 24 min post 4-AP injections (Fig. 11). To further quantify the depth-dependent regions exhibiting differing changes in attenuation coefficient, we averaged the Δμ in three small ROIs (0.2 x 0.2 x 0.2 mm), which were stacked in depth and plotted versus time for all three regions (Fig. 12). With the top ROI exhibited positive Δμ, the middle ROI exhibiting no Δμ, and the bottom ROI exhibiting negative Δμ.

#234156 - $15.00 USD Received 9 Feb 2015; revised 10 Apr 2015; accepted 16 Apr 2015; published 22 Apr 2015
(C) 2015 OSA

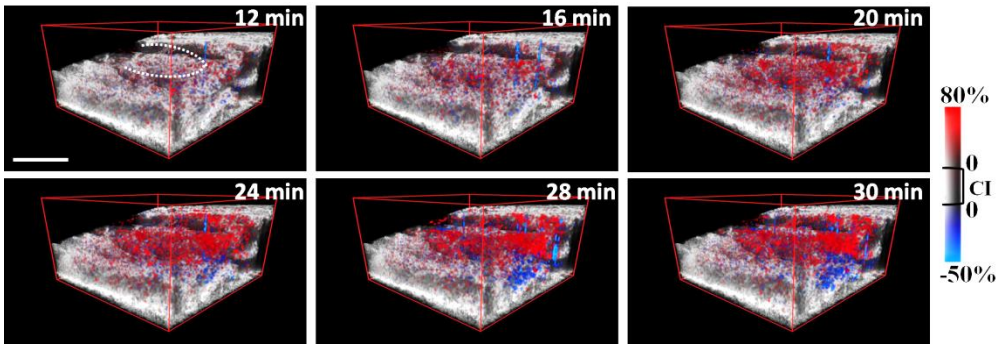

Fig. 11. *f*OCT volumes of the focal seizure 3 x 3 x 2 mm. Color is scaled from black to color saturation at −50% Δμ for blue and 80% Δμ for red representing decreased and increased Δμ respectively. *f*OCT volumes are combined with corresponding attenuation volumes. Time is min post 4-AP injections. Left-back of image: Rostral, right-back of image: Bregma. Dashed line in first frame indicates location of injection pipette. Bar: 1 mm. (see Media 4).

The plot in Fig. 12 shows the average Δμ as a function of time post 4-AP injections in each of the ROIs. The top ROI shows an increase of 15% by the end of the focal seizure (30 min post 4-AP injections) and a significant change as early as 14 min post injections. The middle ROI shows no significant Δμ through focal seizure onset. The bottom ROI shows a decreasing trend, but does not reach a maximum change of −11% until 30 min post 4-AP injections and the change does not become significant until 16 min after the top ROI. The *f*OCT volumes enable the localization of changes in attenuation coefficient of seizing tissue as well as the differentiation between localized regions of cortical tissue exhibiting different spatial and temporal changes in attenuation coefficients during seizure progression.

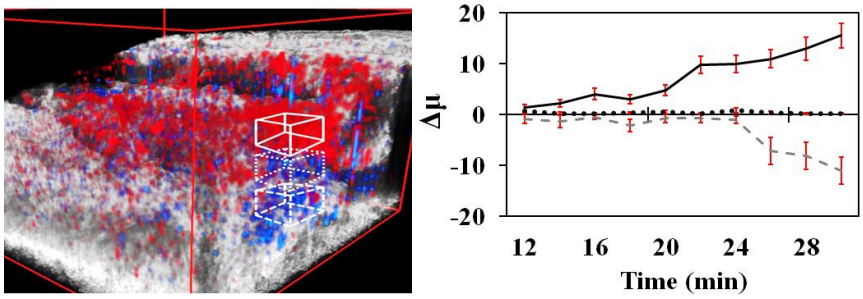

Fig. 12. *f*OCT volume 30 min. post 4-AP injections showing 0.2 x 0.2 x 0.2 mm ROIs for three regions exhibiting increasing (solid), no change (dotted), and decreasing (dashed) Δμ plotted vs. time through focal seizure progression. Error bars are standard error.

3.4 Focal seizure spatiotemporal propagation

Once we verified that we could detect changes in attenuation coefficient locally during a focal seizure, we expanded our imaging field of view to determine if we could visualize how focal seizures propagate from the injection site. To maintain reasonable temporal resolution while increasing the field of view, single volumes of 150 images composed of 512 A-lines were acquired every 40 s. We acquired 5 x 4 x 2 mm volumes with five volumes, acquired prior to the last 4-AP injection. Five baseline volumes providing a *df* of four, allowed for the use of a 0.95 confidence level. The Δμ values were calculated for each volume from which *f*OCT volumes were generated with both blue (negative Δμ) and red (positive Δμ) saturating at ± 30% (Fig. 13). The 4-AP injections were administered 1 mm from the right edge of the volume and 2 mm from bregma with the pipette tip outlined in the first fame in Fig. 13. From

#234156 - $15.00 USD Received 9 Feb 2015; revised 10 Apr 2015; accepted 16 Apr 2015; published 22 Apr 2015
(C) 2015 OSA

the *f*OCT volumes, we were able to identify localized regions that exhibit both positive and negative change in attenuation as well as the spatial propagation from the injection site.

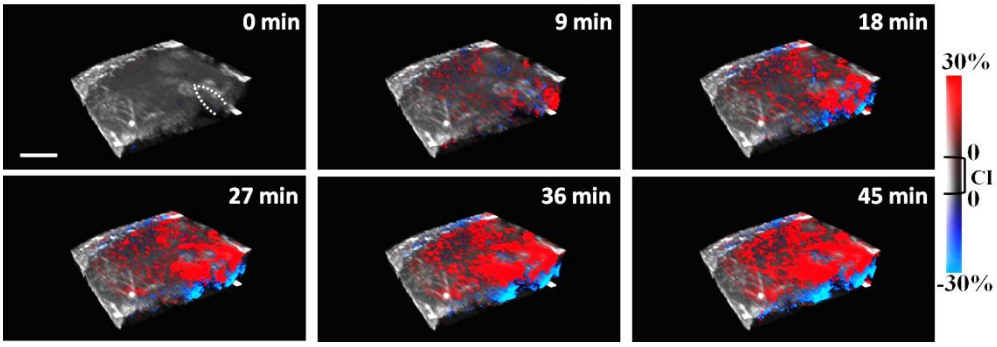

Fig. 13. *f*OCT volumes of focal seizure 5 x 4 x 2 mm. Color is scaled from black to color saturation at –30% Δμ for blue and 30% Δμ for red representing decreased and increased Δμ respectively. *f*OCT volumes are combined with corresponding attenuation volumes. Time is min post 4-AP injections. Dashed line in frame one indicates location of injection pipette. Right back of image: Bregma, front of image: Rostral Bar: 1 mm. (see Media 5).

As a representative of the results for the focal seizure experiments, Fig. 13 shows the *f*OCT volumes minutes post 4-AP injections. Significant changes in attenuation begin to coalesce at the injection site 18 min post injections and continues to propagate radially as the focal seizure progresses resulting in a 1 mm area with maximum change. The results from these experiments also show the layering pattern of changes in attenuation seen previously. We further investigated the layers of cortical tissue showing differing trends in attenuation changes by analyzing them as three distinct layers in time post 4-AP injection (Fig. 14). Layer A was the top 65 μm under the surface, Layer B was the following 52 μm, and Layer C was the following 130 μm and the widths of the layers were selected based on the spatial Δμ patterns observed in the *f*OCT volumes *a posteriori*. Figure 14 shows the *f*OCT data in each of the three layers in time post 4-AP injections as maximum intensity projections (MIPs), which were calculated by collapsing the *z*-axis of each layer in each volume into a 2D *en face* image representing the largest positive or negative Δμ in depth at each pixel. The colors span from white to color saturation at ± 30%.

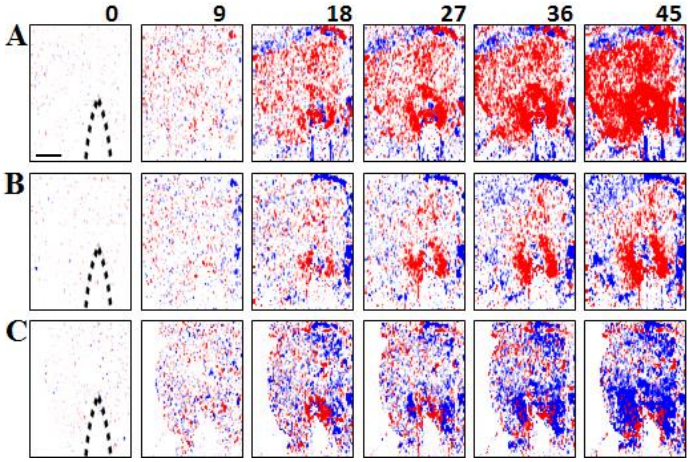

Fig. 14. MIP layered *f*OCT data minutes post 4-AP injections. Layer (A) top 65 μm, layer (B) following 52 μm, and layer (C) following 130 μm. Dashed line in frame one of each layer indicates location of injection pipette. Color spans from white to color saturation at ± 30% Bar: 1mm. (see Media 6).

#234156 - $15.00 USD Received 9 Feb 2015; revised 10 Apr 2015; accepted 16 Apr 2015; published 22 Apr 2015
(C) 2015 OSA

We further investigated the spatiotemporal propagation of the attenuation changes by selecting 0.5 x 0.5 mm ROIs with three consecutively in front of and three consecutively lateral of the injection site (Fig. 15(A)-15(f)). Due to the placement of the pipette with respect to the midline bone, 3 mm of the brain tissue with a hemicraniectomy was to the left of the injection pipette and thus a lateral progression of small ROIs were analyzed in this same direction. We kept the same three layer thicknesses (A, B, and C) and plotted the average Δμ from each of the ROIs as red, black, and blue lines respectively over time post 4-AP injections. In both ROIs (a) and (d) in Fig. 15 there are significant changes in Δμ in layer A and C with a 30-60% increase and a 15-30% decreases during focal seizure propagation. Similarly to the earlier described 4-AP experiments, the decreasing lower layer C did not exhibit a significant change until minutes after the increasing trend. A –5% decrease occurred 34 min post injection, 10 min after a 5% increase in ROI (a). Similarly there is an 8 min delay between the 5% increase and the –5% decrease in ROI (d). Unlike the earlier described 4-AP experiments, however, significant changes also occurred in layer B in some regions (Fig. 15(D)) and followed a similar pattern as layer A except with a more limited propagation radius. As the ROIs step forward and lateral from the injection site, the average Δμ values begin to decrease as seen in the plots in (Fig. 15(B)-15(C) and 15(E)-15(F)) where a maximum of only 10-15% increase and –5-10% decrease occurred with some layers not even exhibiting a greater than ± 1% change.

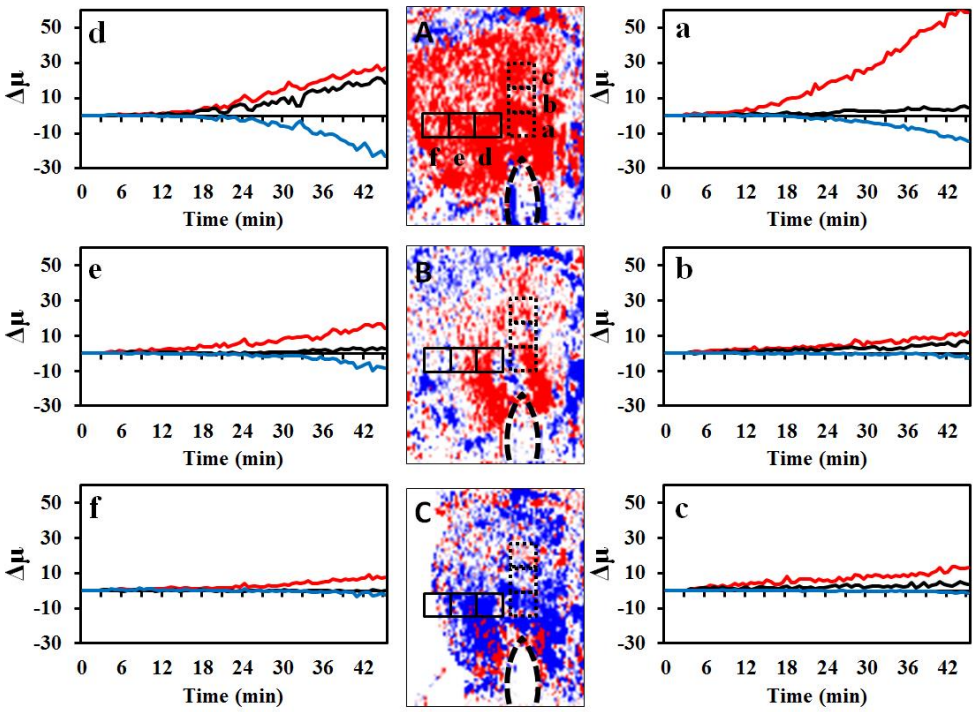

Fig. 15. Consecutive ROIs of average Δμ in front of and lateral of the site of 4-AP injections. Six 0.5 x 0.5 mm ROIs (a-f) were averaged for three layers (A-C). The letter next to the ROI in the top frame refers to the plot with the corresponding letter plotted vs. time post 4-AP injections. Layer A (Red line in plots): top 65 μm, layer B (Black line in plots): following 52 μm, and layer C (Blue line in plots): following 130 μm. Dashed line in each layer indicates location of pipette. MIPs are of the *f*OCT volume 45 min post injections.

#234156 - $15.00 USD Received 9 Feb 2015; revised 10 Apr 2015; accepted 16 Apr 2015; published 22 Apr 2015
(C) 2015 OSA

4. Discussion

In the global and focal seizure experiments, volumetric OCT data was acquired and the percent change in intensity was displayed in three dimensional volumes in time, preserving spatial specificity and accurately conveying the intensity trends occurring during seizure progression. In both seizure models, a large decrease in intensity occurred during seizure progression either throughout the cortical tissue (global model) or localized at the injection site (focal model). These results coincide well with reflectance changes found in previous work with OCT as well as other imaging techniques that are a result of interconnected biological changes in absorption and scattering associated with hemodynamic responses, and neuronal and glial swelling [5,6,8,9,11,19–21,23,25].

In order to better understand the optical properties of the cortical tissue during seizures independent from system intensity levels, we generated volumes of depth-resolved attenuation coefficient values. Previous research observed a depth dependence to the changes in scattering during neural activation [19,21,23,28] and depth-dependent attenuation coefficient volumes provided an even further understanding of the optical properties of cortical tissue by incorporating changes in both absorption and scattering coefficients. The development of the *f*OCT volumes provided high resolution tracking of the spatiotemporal changes of the tissue attenuation values as both global and focal seizures propagate through cortical tissue *in vivo*. In the global seizure model, the *f*OCT volumes revealed significant percent changes in attenuation as well as the heterogeneous distribution of both positive and negative $\Delta\mu$, reflecting the known global nature of seizure progression in the global model. In the focal seizure model *f*OCT volumes, distinct depth-dependent regions exhibiting differing changes in attenuation coefficient were observed. From the analysis of $\Delta\mu$, we were able to clearly differentiate between a global (PTZ) seizure model and focal (4-AP) seizure model and further investigations are necessary to determine the underlying mechanisms that elicited the changes in attenuation during pathologic levels of neural activity.

5. Conclusion

To utilize the spatiotemporal resolution provided by OCT, we developed an analytical method, creating *f*OCT volumes, to display statistically significant changes in the attenuation coefficient of cortical tissue while maintaining high spatial specificity. We were able to differentiate between global and focal seizures through the spatiotemporal pattern of $\Delta\mu$. In the global model, there was a large change in attenuation throughout the tissue, where in the focal model, only a localized region around the injection site showed significant changes in attenuation. The voxel values, which incorporated 30 x 30 x 30 μm of tissue, provided localized visualization of the changes in attenuation coefficient during seizure progression. In addition, we were able to quantify depth-resolved changes in attenuation during seizures as well as track focal seizure propagation with high spatiotemporal resolution. The results from this study demonstrate the potential utility of OCT as a minimally-invasive tool for studying seizure onset and propagation with high spatiotemporal resolution. Future studies will directly compare the temporal performance of seizure detection with *f*OCT versus standard methods (EEG).

Acknowledgements

The authors acknowledge financial support from the following funding sources: the National Institutes of Health (R00EB007241, K08NS059674, R01NS081243), the US National Science Foundation (IGERT: DGE 0903667), and the UC Discovery Grant Program (#213073).